



**Effect of copolymer sequence on structure and relaxation times near a nanoparticle surface**

Journal:	<i>Soft Matter</i>
Manuscript ID	SM-ART-05-2018-000976.R1
Article Type:	Paper
Date Submitted by the Author:	20-Jun-2018
Complete List of Authors:	Trzkovich, Alex; The Ohio State University, William G. Lowrie Department of Chemical and Biomolecular Engineering; Cooper Tire and Rubber Company, Global Technical Center Wendt, Mitchell; The Ohio State University, William G. Lowrie Department of Chemical and Biomolecular Engineering Hall, Lisa; The Ohio State University,



Cite this: DOI: 10.1039/xxxxxxxxxx

## Effect of copolymer sequence on structure and relaxation times near a nanoparticle surface<sup>†</sup>

Alex J. Trazkovich,<sup>\*ab</sup> Mitchell F. Wendt,<sup>a‡</sup> and Lisa M. Hall<sup>\*a</sup>Received Date  
Accepted Date

DOI: 10.1039/xxxxxxxxxx

www.rsc.org/journalname

We simulate a simple nanocomposite consisting of a single spherical nanoparticle surrounded by coarse-grained polymer chains. The polymers are composed of two different monomer types that differ only in their interaction strengths with the nanoparticle. We examine the effect of adjusting copolymer sequence on the structure as well as the end-to-end vector autocorrelation, bond vector autocorrelation, and self-intermediate scattering function relaxation times as a function of distance from the nanoparticle surface. We show how the range and magnitude of the interphase of slowed dynamics surrounding the nanoparticle depend strongly on sequence blockiness. We find that, depending on block length, blocky copolymers can have faster or slower dynamics than a random copolymer. Certain blocky copolymer sequences lead to relaxation times near the nanoparticle surface that are slower than those of *either* homopolymer system. Thus, tuning copolymer sequence could allow for significant control over the nanocomposite behavior.

### 1 Introduction

Because many properties of polymeric materials can be improved by the addition of nanoparticles, polymer nanocomposites are in widespread use in commercial applications and have received significant attention in the scientific community. This has included a large body of simulation work focused on understanding and controlling the molecular scale features of nanocomposite materials.<sup>1–12</sup> A clear picture has developed that near nanoparticle surfaces, there is an interphase in which adsorbed polymer chains have different dynamics, rheology, and typical conformations than in the bulk.<sup>13–21</sup> Because nanoparticles have a high surface area to volume ratio, the addition of even a small volume fraction of particles causes a significant percentage of polymer chains to be incorporated in the interphase region. Thus the overall composite properties are highly dependent on the properties of the interphase and can be predicted as a function of nanoparticle

volume using analytical theories.<sup>22,23</sup> Therefore, understanding and controlling the interactions between polymer chains and nanoparticle surfaces is key to predicting and tuning bulk material properties.

A critical factor that helps determine properties of the interphase is the polymer–filler interaction strength, which is dependent on the specific polymer and nanoparticle surface chemistry and can be further adjusted by functionalizing the nanoparticle surface. Favorable polymer–filler interactions are key to ensuring good nanoparticle dispersion; when interactions are unfavorable, nanoparticles have the tendency to aggregate due to entropic depletion effects, which usually has an adverse effect on the mechanical properties of the resulting composite. Therefore, for many common systems, polymer–filler interactions are favorable. This allows polymers to adsorb on the surface of the nanoparticle, and the dynamics of the polymers adsorbed on the nanoparticle are slowed.<sup>24–29</sup> This raises the local glass transition temperature in the interphase, and in more highly-loaded systems, the glass transition temperature of the overall composite can be noticeably increased.<sup>30–33</sup> It is also possible to obtain an interphase region with faster dynamics than the bulk by selecting components such that the interaction is unfavorable<sup>16</sup>, which has the effect of lowering glass transition temperatures.<sup>33–35</sup>

One class of systems that has been the subject of increased attention in recent years consists of nanoparticles incorporated into blocky copolymer systems.<sup>36</sup> In these systems, one component of the copolymer may interact more favorably with the nanoparticle than the other. These systems have been the subject of several simulation studies focused on nanoparticle dispersion in

<sup>a</sup> William G. Lowrie Department of Chemical and Biomolecular Engineering, The Ohio State University, USA. Fax: 614 292 3769; Tel: 614 292 4000; E-mail: trazkovich.1@osu.edu, hall.1004@osu.edu

<sup>b</sup> Global Technical Center, Cooper Tire & Rubber Company, Findlay, USA.

<sup>†</sup> Electronic Supplementary Information (ESI) available: [The ESI includes the following additional figures:

- S1: A monomer-nanoparticle and B monomer-nanoparticle pair distribution functions,  $g_{AN}(r)$  and  $g_{BN}(r)$
- S2: Chain end-to-end orientations as a function of distance from the nanoparticle
- S3: Bond vector orientations as a function of distance from the nanoparticle

]. See DOI: 10.1039/b000000x/

microphase-separated block copolymers<sup>37–41</sup> as well as the effect of grafted copolymer chain sequence on nanoparticle interactions and self-assembly.<sup>42–44</sup> Sequence effects have also been extensively studied in the context of biological systems, where amino acid sequence can play a critical role in the interaction between proteins and nanoparticles.<sup>45–47</sup> However, relatively little simulation work has focused specifically on properties of the copolymer–nanoparticle interphase.

In a recent study,<sup>48</sup> Chen and colleagues simulated regular multiblock copolymer chains of hydrophobic and hydrophilic monomers adsorbed to a hydrophobic nanoparticle. The authors focused on the formation of micelle-like structures of hydrophobic monomers, which could either form adsorbed on part of a nanoparticle or surrounding the nanoparticle. The authors found that with all pairwise interactions equal to  $\epsilon$  except for the hydrophobic–hydrophobic interactions, micelles preferentially formed adjacent to the nanoparticle when the interaction strength between the hydrophobic monomers was above a critical threshold close to  $\epsilon$ . In another study<sup>49</sup>, Martin et al. modeled a nanoparticle grafted with copolymer chains composed of alternating blocks of equal length. When one of the monomer types had a higher affinity for the nanoparticle, chain conformations around the nanoparticle were shown to depend on the length of the blocks used in the copolymer sequence. Generally, as block length increased, the average distance between the nanoparticle and the monomer type with higher affinity for the nanoparticle decreased while the average distance of the less adsorbing monomer type increased; however, some systems did not follow this expected behavior, depending on the strengths of the various monomer–monomer interactions as well as which block (high or low affinity) was grafted to the nanoparticle.

Prior simulation studies of copolymer nanocomposites have typically considered unfavorable interactions between unlike monomers; however, a body of theoretical work on copolymer–nanoparticle systems from the Schweizer group considered monomers that differ only in their nanoparticle interactions, as we do here. Specifically, they showed that even when the only chemical difference between the monomers is the strength of their interaction with the nanoparticles (so the bulk behaves as a homopolymer with no tendency to microphase separate), copolymer structure in the vicinity of nanoparticles depends dramatically on the copolymer sequence.<sup>50–52</sup> An adsorbed monomer layer was found to form around each nanoparticle (in which there was an increased concentration of adsorbing monomers), and the width of this phase increased with copolymer block length. Additionally, in systems with multiple nanoparticles, nanoparticles that were significantly smaller than the block length were found to have a much higher tendency to aggregate.

Here, we now use molecular dynamics simulations to show how copolymer sequence impacts interphase *dynamics* as well. This topic was not addressed in the theoretical work described above. However, a recent experimental study by Helal et al. presented some evidence that copolymer sequence impacts interfacial glass transition temperature; in a nanocomposite consisting of clay nanoparticles in polystyrene-*b*-poly(ethylene-co-butylene)-*b*-polystyrene, the glass transition temperature in the

interphase was found to depend on the length of the polystyrene blocks.<sup>53</sup>

We have recently performed a brief simulation study using a model where the only chemical difference between the two monomer types was their strength of adsorption to a nanoparticle, and we showed that copolymer sequence affects not only local structure and qualitative conformations (Figure 1) around the nanoparticle but also end-to-end relaxation times, which tended to increase near the nanoparticle with increasing copolymer block size.<sup>54</sup> In the current work, we use the same model to study a larger set of copolymer sequences, and we examine the effect of copolymer sequence on interphase dynamics by measuring end-to-end autocorrelation function, bond-vector autocorrelation function, and self-scattering function relaxation times. All of these quantities are measured as a function of distance from the surface of the nanoparticle to show how copolymer sequence impacts the width and properties of the polymer–nanoparticle interphase.

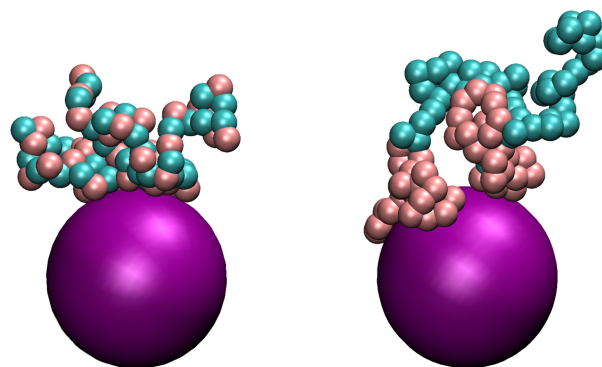


**Fig. 1** Representative snapshots of selected polymers from two simulated systems. Pink beads adsorb more strongly to the nanoparticle (purple) than cyan beads.

## 2 Methods

Our simulations use the standard Kremer-Grest bead-spring model.<sup>55,56</sup> Polymers are linear, freely-jointed chains of  $N = 100$  coarse-grained monomer beads. Therefore, the system is only lightly entangled; standard Kremer-Grest chains of this length have fewer than two entanglements per chain on average (note that we include the attractive part of the LJ interaction and our systems are slightly denser than the standard repulsive Kremer-Grest system).<sup>57</sup> 400 chains are placed in a cubic simulation box along with a single nanoparticle, and periodic boundary conditions are applied. Copolymer chains contain an equal number of A and B monomers, which may be arranged randomly or in one of six regular alternating block sequences of the form  $[A_xB_x]_y$ , with  $x$  equal to 1, 2, 5, 10, 25, or 50 depending on the system and  $y$  equal to  $100/(2x)$ . Thus,  $x$  is the block length, which we call  $B_L$ ; we refer to these systems as “ $B_L = x$ ”. Although regular multiblock copolymer sequences are difficult to synthesize experimentally, researchers have had success producing such sequences by successively reacting multiple carefully-prepared functionalized diblock copolymers.<sup>58</sup>

Chain sequences in the random copolymer system are individually generated by randomizing the order of a sequence containing 50 A and 50 B monomers; thus, individual chains in the random copolymer may have different sequences, although they are restricted to contain 50% of each monomer type. In the specific set of random sequences used in this work, the average length of a block containing a randomly chosen B monomer was 2.99, the average length of the longest B block on each chain was 5.86, and the length of the longest single B block in the system was 13 (note that, unlike the two previous quantities, the length of the longest B block would be expected to increase with system size). Figure 2 depicts a schematic of several of our copolymer systems. We also simulate homopolymer A and homopolymer B systems for comparison.

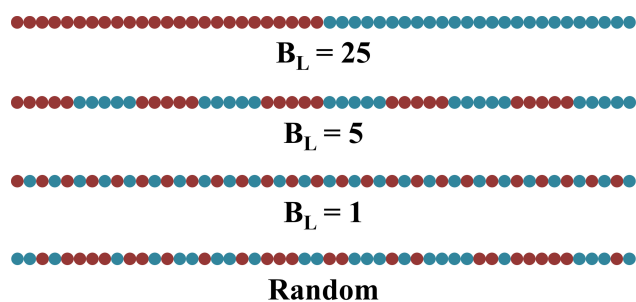


**Fig. 2** Schematic of some of the copolymer block sequences used in this work. Each segment shows half of a  $N = 100$  polymer chain.

We use  $\sigma$ ,  $\epsilon$ , and  $m$  as our reduced units of length, energy, and mass respectively. All monomers have a mass equal to  $1.0m$ . The reduced unit of time is therefore  $\tau = \sigma(m/\epsilon)^{1/2}$ .

Bonded monomers are coupled by Finite Extensible Nonlinear Elastic (FENE) potentials:

$$U_{\text{FENE}} = \begin{cases} -\frac{1}{2}kR_0^2 \ln \left[ 1 - \left( \frac{r}{R_0} \right)^2 \right] & r \leq R_0 \\ 0 & r > R_0 \end{cases}, \quad (1)$$

where  $r$  is the distance between the bonded monomers,  $R_0$  is the bond cutoff, set to  $1.5\sigma$ , and  $k$  is a constant that sets the strength of the bond, set to  $30\epsilon/\sigma^2$  to prevent chain crossing or scission.<sup>56</sup>

Monomer–monomer pairwise interactions are modeled by a standard cut-off and shifted Lennard-Jones (LJ) potential,

$$U_{\text{LJ},ij} = \begin{cases} 4\epsilon_{ij} \left[ \left( \frac{\sigma_{ij}}{r} \right)^{12} - \left( \frac{\sigma_{ij}}{r} \right)^6 \right] + \delta & r \leq r_c \\ 0 & r > r_c \end{cases}, \quad (2)$$

where  $\epsilon_{ij}$  is the strength of the interaction and  $\sigma_{ij}$  is the length scale of the interaction between monomer types  $i$  and  $j$ .  $r_c$  is the cutoff distance, which is set to  $2.5\sigma_{ij}$  for non-bonded monomers and  $2\frac{1}{2}\sigma_{ij}$  for bonded monomers.  $\delta$  is a vertical shift factor chosen so that  $U_{\text{LJ}}(r_c) = 0$ . All monomer sizes and monomer–monomer LJ potential interaction strengths are equal, so that  $\sigma_{\text{AA}} = \sigma_{\text{AB}} = \sigma_{\text{BB}} = 1.0\sigma$  and  $\epsilon_{\text{AA}} = \epsilon_{\text{AB}} = \epsilon_{\text{BB}} = 1.0\epsilon$ .

The effective diameter of the nanoparticle,  $\sigma_{\text{N}}$ , is set to  $10.0\sigma$ . The nanoparticle–monomer interactions follow a radially shifted LJ potential,

$$U_{\text{NM}} = \begin{cases} \infty & r - \Delta \leq 0 \\ 4\epsilon_{\text{NM}} \left[ \left( \frac{\sigma}{r - \Delta} \right)^{12} - \left( \frac{\sigma}{r - \Delta} \right)^6 \right] + \delta & 0 < r - \Delta \leq r_c \\ 0 & r - \Delta > r_c \end{cases}, \quad (3)$$

where the shift factor  $\Delta = (\sigma_{\text{N}} - \sigma)/2 = 4.5\sigma$ . This potential has been used in several coarse-grained simulation studies of polymer–nanoparticle composites.<sup>2,14,59</sup> The strength parameter  $\epsilon_{\text{NM}}$  varies with monomer type, M; A monomers have the same affinity for the nanoparticle as for other monomers ( $\epsilon_{\text{NA}} = 1$ ), while B monomers are strongly attracted to the nanoparticle ( $\epsilon_{\text{NB}} = 5$ ). This is the only chemical difference between the monomers. Note that since the nanoparticle is larger than the monomers,  $\epsilon_{\text{NA}} = 1$  is effectively a slightly repulsive interaction: as a monomer moves to the surface of the nanoparticle from the polymer bulk, it loses multiple interactions with other monomers but gains only a single interaction with the nanoparticle. The strength of  $\epsilon_{\text{NB}}$  was chosen to produce a significant difference between the two monomer types while still allowing adsorbed polymers to desorb over computationally accessible timescales.

We ran MD simulations using the open-source package LAMMPS with the default equations of motion<sup>60</sup> and a timestep  $\delta t = 0.01$ . Initial chain conformations are random walks except that they are excluded from the nanoparticle. After an initial soft pushoff phase to eliminate polymer overlap, we ran an equilibration simulation in the isobaric-isothermal (NPT) ensemble. A Nosé-Hoover thermostat (damping parameter 1.0) held the reduced temperature at 1.0, and a Nosé-Hoover barostat (damping parameter 10.0) held the reduced pressure at 0. The NPT equilibration phase ran for  $200,000\tau$ , which was sufficient for the root mean squared displacement ( $16.8\sigma$ ) to be more than three times as long as the average radius of gyration (approximately  $5.1\sigma$ ). Additionally, this was 10 times the bulk end-to-end relaxation time and more than 5 times longer than the longest end-to-end relaxation time observed near the nanoparticle surface. We also manually confirmed that all polymer chains which were initially absorbed to the nanoparticle desorbed at some point during the equilibration phase.

Data was collected during a production run performed in the microcanonical (NVE) ensemble. The volume was fixed at the average volume from the final  $10,000\tau$  (one million timesteps) of the NPT equilibration phase. A brief further equilibration phase of  $50,000\tau$  was performed after switching to NVE and before saving any data for analysis. After equilibration in NVE, The length of each side of the cubic simulation box was approximately  $36\sigma$ , so the distance from the nanoparticle center to the nearest edge of the periodic cell was approximately  $18\sigma$ . By all measures considered, the polymer properties were within 2% of the bulk values before the edge of the box in every system considered. Specifically, this 2% threshold was met at approximately  $12\sigma$  for radii of gyration and the end-to-end autocorrelation function relaxation time,  $9\sigma$  for bond vector autocorrelation function and self-

intermediate scattering function relaxation times, and  $17\sigma$  for the A and B monomer-nanoparticle pair distribution function peak heights.

Data was saved for analysis according to three different schemes depending on the quantities of interest. For calculating static quantities including the radial pair distribution function and radius of gyration, data was saved every  $100\tau$  for  $200,000\tau$ . For calculating self-intermediate scattering and bond vector autocorrelation functions, data was saved at powers of  $\sqrt{2}$  (rounded to the nearest integer) in 100 separate trajectories whose initial configurations were separated by  $1,000\tau$ , well past the relevant relaxation times. For calculating the end-to-end autocorrelation function, data was saved at every power of  $\sqrt{2}$  in 200 separate trajectories whose initial configurations were separated by  $50,000\tau$ , also past the relevant relaxation time.

### 3 Results

The structure of the interphase of monomers around the nanoparticle is quantified by the monomer-nanoparticle pair distribution function,  $g_{MN}(r)$ , the relative probability of finding a monomer of type M at distance  $r$  from the nanoparticle compared to the probability in the bulk. We use the index P to refer to all monomers, and recall that A refers to nonadsorbing monomers and B refers to adsorbing monomers. We also calculate  $g_{BN}(r)/g_{PN}(r)$ , the ratio of the B-nanoparticle pair distribution function to the overall monomer-nanoparticle radial pair distribution function, which is equivalent to the probability that a randomly chosen monomer at distance  $r$  is type B (Figure S1 in the Electronic Supplementary Information<sup>†</sup> reports this same data in terms of the more standard A-nanoparticle and B-nanoparticle pair distribution functions). As shown in Figure 3(a), radial ordering for the copolymer systems generally falls between that of A homopolymer and B homopolymer systems. All copolymer systems (which include 50% B) have noticeably higher first, second, and third peaks in  $g_{PN}(r)$  versus the A homopolymer due to monomer adsorption. These peaks intensify with block length, and the systems with  $B_L \geq 10$  are nearly indistinguishable from the pure B system.

The ratio  $g_{BN}(r)/g_{PN}(r)$  is reported in Figure 3(b); all systems exhibit a phase around the nanoparticle where the fraction of B monomers is above 0.5, and for  $B_L \geq 10$ , this phase is nearly pure B. The width of this phase increases with the block length. Surrounding this first phase, most of the systems exhibit a second region where the fraction of A monomers is above 0.5, although this effect is minimal in the random and  $B_L = 50$  systems. In the  $B_L = 25$  system, this secondary A-dominant phase extends to about  $14\sigma$  from the center of the nanoparticle (the plot has been cropped for visual clarity). After this secondary A-dominant phase, all systems' concentrations converge to the bulk value (equal concentrations of A and B monomers). Near the nanoparticle, the fraction of B monomers in the random copolymer system most closely resembles that of the  $B_L = 5$  system. This is consistent with the average length of the longest B block in each chain in the random system and fact that the longer B blocks will tend to preferentially aggregate around the nanoparticle. Out of all the systems, the random copolymer system converges to equal concentrations of A and B monomers over the shortest length

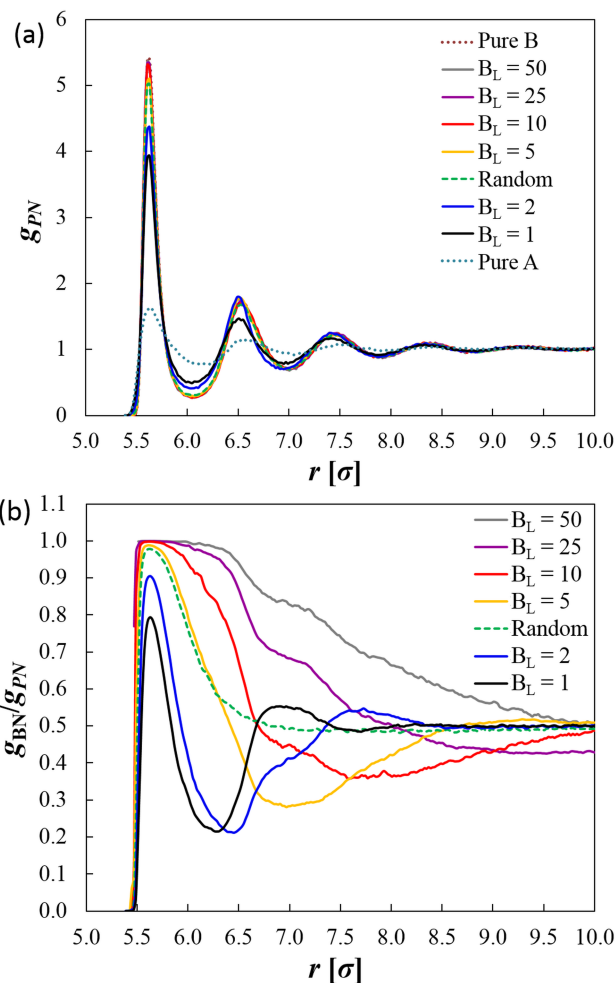


**Fig. 3** (a)  $g_{PN}(r)$ , the monomer-nanoparticle radial pair distribution function for the copolymer systems as well as the two homopolymer systems, as labeled, for comparison. (b)  $g_{BN}(r)/g_{PN}(r)$ , the fraction of monomers at distance  $r$  that are type B, for the copolymer systems, as labeled.

scale; this is likely because in the random system, the composition varies within and between chains, and a long B block adsorbed to the nanoparticle may not be adjacent to a long A block, so the secondary A dominant phase is not present.

The fraction of B monomers yields one way to measure the width of the static interphase. For this purpose, we define the surface of the nanoparticle as  $\sigma_N/2 = 5\sigma$ , and we define the interphase as extending from the nanoparticle out to the last point where the fraction of B monomers differs from the bulk value of 0.5 by more than 5%. This yields interphases with widths of  $1.5\sigma$  for the random copolymer system,  $2\sigma$  for  $B_L = 1$ ,  $3\sigma$  for  $B_L = 2$ ,  $3.5\sigma$  for  $B_L = 5$ ,  $4\sigma$  for  $B_L = 10$ ,  $7\sigma$  for  $B_L = 25$ , and  $4\sigma$  for  $B_L = 50$ . Note that these values are somewhat sensitive to the cutoff threshold used.

To characterize polymer chain behavior in the interphase, we first examine the radius of gyration ( $R_g$ ) as a function of distance from the nanoparticle center (see Figure 4). Specifically, based on each chain's center of mass (COM), polymers were assigned to concentric spherical shells around the nanoparticle.

Far from the nanoparticle, all systems have very similar  $R_g$  since

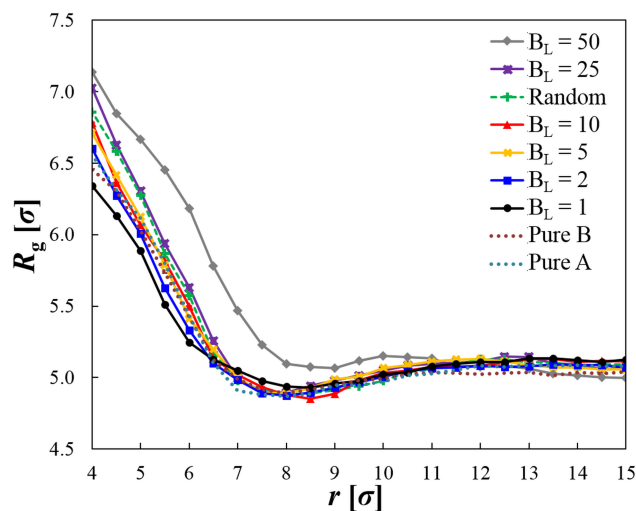


**Fig. 4** Average radius of gyration of polymer chains as a function of distance from the center of the nanoparticle. Polymers are assigned to shells as described in the text, and shells are centered at the indicated radius and have a width of  $0.5\sigma$ . Adequate statistics were not obtained to report on the rare cases where a polymer's center of mass resides at  $r < 3.75\sigma$

there is no chemical difference between the monomers in the bulk. Between about  $r = 11\sigma$  and  $r = 8\sigma$ ,  $R_g$  decreases slightly with proximity to the nanoparticle, then for  $r < 8\sigma$ ,  $R_g$  increases sharply as  $r$  decreases. In this latter region,  $R_g$  tends to increase with  $B_L$  in the multiblock copolymer systems while the results of the two homopolymer systems are very similar. Notably, for  $B_L = 1$ ,  $R_g$  is significantly lower than either homopolymer system throughout this entire region, while for  $B_L \geq 25$ ,  $R_g$  is significantly higher. The random copolymer system most closely resembles the  $B_L = 25$  system. The  $B_L = 50$  system has a significantly higher  $R_g$  than any of the other systems out to a radius of  $10\sigma$ ; since the  $B_L = 50$  chains are diblock copolymers, the chain conformation is more extended when the B block is adsorbed and the A block is outside the B-dominant phase surrounding the nanoparticle. All the other sequences allow for multiple B blocks on the same chain to adsorb on the nanoparticle, making a more compact conformation.

To study the effect of copolymer sequence on chain dynamics in the polymer–nanoparticle interphase, we calculate vector autocorrelation functions. Specifically, we extract chain- and bond-scale relaxation times by fitting relevant vector autocorrelation functions with a stretched exponential model,<sup>2</sup>

$$\frac{\langle R(t) \cdot R(0) \rangle}{\langle R(0)^2 \rangle} \approx e^{-\left(\frac{t}{\tau_R}\right)^{\beta_R}}, \quad (4)$$

where  $R$  is the relevant vector at time  $t$ ,  $\tau_R$  represents the mean relaxation time of vector  $R$ , and  $\beta_R$  is a stretching parameter related to the width of the relaxation time distribution.

When  $R$  is the polymer chain end-to-end vector,  $R_{ee}$ , the left side of Equation 4 is the end-to-end autocorrelation function, and  $\tau_{ee}$  and  $\beta_{ee}$  are parameters describing the mean and width of the distribution of the end-to-end relaxation times. When  $R$  is the

vector between adjacent bonded monomers,  $R_{bv}$ , the left side of Equation 4 is the bond vector autocorrelation function, and  $\tau_{bv}$  and  $\beta_{bv}$  describe the mean and width of the distribution of bond vector relaxation times. In this study,  $\tau_{ee}$  and  $\tau_{bv}$  are of particular interest because they describe the characteristic timescale of chain and bond relaxation, respectively.

Prior work has used the end-to-end autocorrelation function to characterize interphase polymer dynamics as a function of distance from both flat surfaces<sup>18</sup> and nanoparticles.<sup>28</sup> Using a similar approach, we divide the system into a series of concentric shells centered on the nanoparticle and assigning each polymer the shell that contains the chain's COM at the middle frame of the autocorrelation window. Polymers may move between shells during the course of the autocorrelation window, but this effect is reduced by truncating the trajectories at  $\sqrt{2}^{44}$  timesteps (approximately  $42,000\tau$ ), which is approximately  $2\tau_{ee}$  of the bulk system. The data from each shell is fitted with the stretched exponential model to extract  $\tau_{ee}$  and  $\beta_{ee}$ .  $\beta_{ee}$  was found to be close to 0.55 and relatively independent of copolymer sequence and distance from the nanoparticle. On the other hand,  $\tau_{ee}$  was found to depend significantly on both copolymer sequence and proximity to the nanoparticle, as shown in Figure 5.

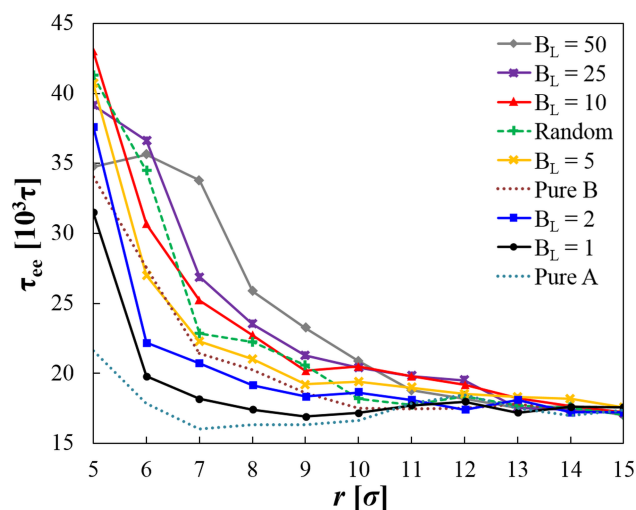


**Fig. 5** End-to-end relaxation times of various copolymer and homopolymer systems, as labeled, as a function of distance from the nanoparticle surface. Polymers are assigned to shells as described in the text, and shells are centered on the indicated radius and have a width of  $1\sigma$ . Measurement error increases with proximity to the nanoparticle because fewer polymers reside in closer shells. A 90% confidence interval of the measurement is approximately  $\pm 2.5 \cdot 10^3 \tau$  at  $5\sigma$ ,  $\pm 1.5 \cdot 10^3 \tau$  at  $6\sigma$ ,  $\pm 1 \cdot 10^3 \tau$  at  $8\sigma$ , and  $\pm 0.5 \cdot 10^3 \tau$  at  $15\sigma$ . Adequate statistics were not obtained to report on the rare cases where a polymer's center of mass resides at  $r < 4.5\sigma$ .

In the A homopolymer system, chain relaxation timescales decrease slightly in the vicinity of the nanoparticle, which is consistent with other work that has shown this effect for nanocomposite systems with slightly repulsive polymer–nanoparticle interactions. The exception is at the closest reported shell, where the confining effect of the nanoparticle surface appears to slightly outweigh the effect of the repulsive interaction. In all other systems, chain relaxation timescales increase with proximity to the

nanoparticle. In the blocky copolymer systems, increasing block length tends to increase relaxation times at a given distance from the nanoparticle. The lengthscale over which relaxations are slowed also appears to increase with block length. The interphase chain relaxation times of the random copolymer system are similar to those of the  $B_L = 5$  and  $B_L = 10$  systems.

In contrast to the overall trend, in the closet shell reported, the  $B_L = 50$  system exhibits statistically significantly smaller relaxation times than several other systems with shorter block lengths. In this system, the chain COM is rarely in the shell closest to the nanoparticle surface because of the tendency of chains to orient with their A blocks far from the surface. Chains that happen to be in an unfavorable conformation with COM near the surface will relatively quickly reorient to a more favorable orientation.

Interestingly, above a threshold of approximately  $B_L = 5$ , the interphase chain relaxation times are slower than for the B homopolymer system despite the fact that the B homopolymer system contains twice as many adsorbing B monomers as the copolymer systems. This may be because, in the copolymer systems, there is an energy barrier associated with swapping an adsorbed B block with another B block on the same chain, and this energy barrier increases with the length of the non-adsorbing A blocks that separate the B blocks. In the B homopolymer system, adsorbing chain segments may be swapped without experiencing this barrier.

Chain relaxation times provide another method to characterize the interphase, this time in terms of dynamics. As before, we define the surface of the nanoparticle as  $5\sigma$ , and we now define the interphase as extending from the nanoparticle out to the last point where  $\tau_{ee}$  differs from the bulk value of  $17.3 \times 10^3 \tau$  by more than 10%. This yields interphases with approximate widths of  $9\sigma$  for the random copolymer system,  $1\sigma$  for  $B_L = 1$ ,  $3\sigma$  for  $B_L = 2$ ,  $5\sigma$  for  $B_L = 5$ ,  $7\sigma$  for  $B_L = 10$ ,  $7\sigma$  for  $B_L = 25$ ,  $5\sigma$  for  $B_L = 50$ ,  $3\sigma$  for homopolymer B, and  $0\sigma$  for homopolymer A.

This analysis of interphase widths (and, in general, all the analysis of local end-to-end vector relaxation times) is confounded by the fact that  $\tau_{ee}$  is a property of the entire polymer chain, so it represents a physical process that is distributed over an area significantly wider than the width of a single shell. Therefore, the analysis above should be treated only as a rough view of the progression of interphase dynamics rather than a precise measurement of local properties.

To provide a more localized description of relaxation, we also measure the bond vector autocorrelation function. Orientational relaxation of bonds has been similarly studied by others,<sup>61</sup> including as a function of distance from a nanoparticle surface.<sup>28,62</sup> Importantly, this characterizes dynamics on a length scale that is close to the width of a single shell.

Figure 6 reports  $\tau_{bv}$  as a function of distance from the nanoparticle surface for each of the systems studied. In this case, fits to determine  $\tau_{bv}$  are performed using data for  $t \leq 10\tau$ , during which time the mean-squared displacement of the monomers is less than 1, meaning that the majority of monomers should remain in or near the shell to which they are assigned during the analysis time. As with the end-to-end relaxations, bond-scale relaxation times in the B homopolymer and all copolymer systems

increase with proximity to the nanoparticle, although the length scale over which this effect occurs is shorter than for the chain relaxations. Compared to the end-to-end relaxations, there is relatively less variation between the copolymer systems, with the behavior all of the copolymer systems strongly resembling that of the B homopolymer for  $r \geq 7$ .

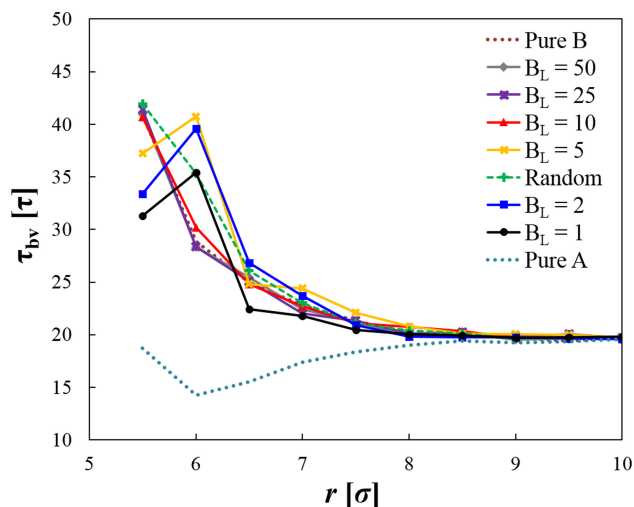


**Fig. 6** Bond vector relaxation times as a function of distance from the nanoparticle surface for the various copolymer and homopolymer systems, as labeled. Shells are centered at the indicated distance and have a width of  $0.5\sigma$ , and bonds are assigned to shells as described in the text. Measurement error increases with proximity to the nanoparticle because fewer bonds reside in closer shells. A 90% confidence interval of the measurement is approximately  $\pm 1\tau$  at  $5.5\sigma$ ,  $\pm 0.5\tau$  at  $7\sigma$ , and  $\pm 0.1\tau$  at  $10\sigma$  and above.

Bond relaxation very close to the nanoparticle depends primarily on the local percentage of adsorbing monomers (Figure 3b). For  $B_L \leq 10$ , bond relaxations in the closest shell ( $r = 5.5\sigma$ ) increase with  $B_L$ , as does the fraction of B monomers. For  $B_L \geq 10$ , the relaxation times plateau at nearly the same value as the B homopolymer system; this corresponds to the copolymer block length threshold above which the fraction of B monomers in the phase adjacent to the nanoparticle's surface is nearly indistinguishable from 1. However, the random copolymer system exhibits bond relaxations in the first shell that are nearly equivalent to those of the longest block length copolymer systems despite having a locally adsorbed B-dominant phase that is less pure than that of the  $B_L = 5$  system. In the  $r = 6\sigma$  shell, several of the shorter block length systems as well as the random system exhibit significantly slower bond relaxations than the B homopolymer system. This may be attributable to the very sharp transitions in the percentage of B monomers observed at approximately that distance from the nanoparticle in the  $B_L \leq 5$  systems; A-B bonds that are aligned across that boundary may be disproportionately slow to relax as a result of the sharp phase transition (the orientation of bonds with respect to the nanoparticle is reported in the Electronic Supplementary Information<sup>†</sup>, Figure S3).

In contrast to what is seen with the chain relaxation data, the apparent interphase width according to bond relaxation is relatively independent of copolymer sequence, with all systems con-

verging to the bulk value approximately the same distance from the nanoparticle surface. For several systems, this is a shorter lengthscale than the convergence of either the composition or the chain relaxation times. Note that this is, in large part, a consequence of our particular model, which defines the two monomer types as identical except for their interactions with the nanoparticle. If inter-monomer interactions were adjusted to vary with monomer type, then it is likely that the interphase width according to local dynamic properties such as bond relaxations would be more similar to the interphase width according to composition. In contrast, in our system, the bond relaxation times converge to the bulk value after about  $2.5\sigma$  from the nanoparticle surface, which is the cutoff distance of the monomer–nanoparticle interaction potential, the distance out to which monomer-scale dynamics are directly impacted by their interaction with the nanoparticle. In contrast, in the case of chain-scale relaxation times, apparent interphase effects can persist out to distances significantly beyond the  $2.5\sigma$  cutoff because polymers whose chain centers are beyond the cutoff distance may still contain some monomers which are much closer to the nanoparticle. In fact, the widest interphases according to chain relaxation times were seen to be about  $7\sigma$ , which is approximately the sum of the cutoff distance and the radius of gyration.

To characterize local monomer mobility, we use the self-intermediate scattering function  $F_S(\mathbf{k}, t)$ , defined as

$$F_S(\mathbf{k}, t) = \frac{1}{N} \left\langle \sum_j \exp[i\mathbf{k} \cdot (\mathbf{r}_j(t) - \mathbf{r}_j(0))] \right\rangle, \quad (5)$$

where  $\mathbf{r}_j(t)$  is the position of monomer  $j$  at time  $t$ ,  $N$  is the number of monomers in the shell, and  $\mathbf{k}$  is a wave vector.

In contrast to the bond vector autocorrelation, which measures local bond reorientation, the self-intermediate scattering function measures monomer translation and has previously been used by Ghanbari et al. to characterize the polymer–nanoparticle interphase.<sup>24</sup> It also effectively encodes the same information as the mean-squared displacement, which was used by Ndoro and colleagues in a similar context.<sup>28</sup> Note that while this formulation of the self-consistent scattering function is omni-directional, treating movement in all directions as equivalent, it would also be possible in future work to consider  $\mathbf{k}$  vectors normal to the nanoparticle surface in order to characterize monomer motion towards or away from the nanoparticle.

To characterize the interphase using  $F_S(\mathbf{k}, t)$  results, we apply a similar treatment as for the vector autocorrelations: we assign monomers to shells based on their locations at  $t/2$  and then fit the ensemble average of each shell with a stretched exponential model (right side of Equation 4). We focus on changes in  $\tau_{F_S}(\mathbf{k}, t)$ , the characteristic relaxation time of  $F_S(\mathbf{k}, t)$ , across systems. As with the analysis of bond vector relaxation, fits to determine  $\tau_{F_S}(\mathbf{k}, t)$  are performed using data for  $t \leq 10\tau$ . Figure 7 plots these relaxation times as a function of distance from the nanoparticle for  $\mathbf{k} = 2\pi\sigma^{-1}$ , corresponding to the monomer diameter length scale.

The results for all systems exhibit an oscillatory behavior that coincides with the fluctuations in the monomer–nanoparticle pair

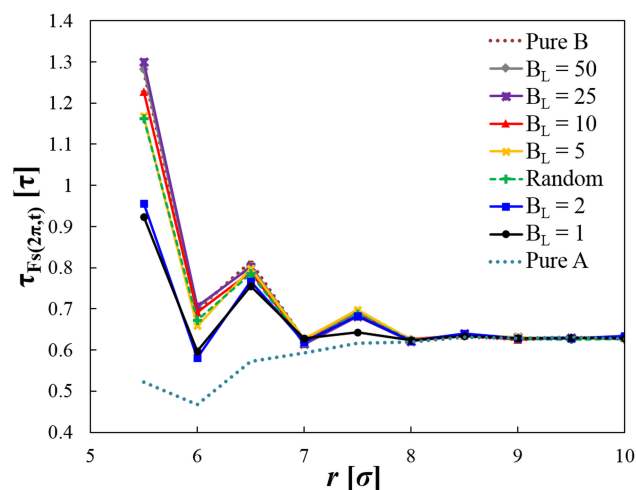


**Fig. 7** Relaxation times of the self-intermediate scattering function at  $|\mathbf{k}| = 2\pi$ , reported as a function of distance from the nanoparticle surface for the various copolymer and homopolymer systems, as labeled. Monomers are assigned to shells as described in the text, and shells are centered at the indicated distance and have width of  $0.5\sigma$ . Although measurement error increases with proximity to the nanoparticle because fewer monomers reside in closer shells, a 90% confidence interval of the measurement is less than  $\pm 0.02$  at all radii.

distribution function seen in Figure 3(a); monomers in locations of high relative density due to structural ordering around the nanoparticle are seen to be less mobile over short timescales than the fewer monomers found in areas of low density at the middle of the time window (these monomers may have been in the process of moving between higher density locations during the time window). Except in the A homopolymer system, monomer-scale motions slow with proximity to the nanoparticle. Generally,  $F_S(\mathbf{k}, t)$  relaxation times for the copolymer systems fall between those of the A homopolymer and B homopolymer systems. Relaxation times in the blocky systems are seen to increase with block length, with the relaxation times of the  $B_L = 25$  and  $B_L = 50$  systems being nearly indistinguishable from the homopolymer B system. The behavior of the random copolymer system is most similar to that of the  $B_L = 5$  system.

The apparent interphase width according to the self-consistent scattering function is approximately  $2.5\sigma$  and is relatively independent of copolymer sequence. As with the interphase width according to bond-vector relaxation times (see discussion above), this is likely linked to the cutoff distance of the monomer–nanoparticle interaction potential.

## 4 Conclusions

Using a series of AB copolymer sequences and a simple coarse-grained model where the only chemical difference between the A and B monomer is their strength of attraction to a nanoparticle, we examined the effect of copolymer sequence on the structure and dynamic properties of the polymer–nanoparticle interphase. We compared the results from the copolymer systems to homopolymer A and homopolymer B systems, finding that, within the range of copolymers studied, adjusting sequence could tune the interphase to take on a range of properties between extremes

bounded by the homopolymer A and homopolymer B systems. Moreover, depending on the interphase property of interest, in some cases it is possible to produce interphase behavior that is outside the regions bounded by pure A and pure B systems. This is most clear in the case of end-to-end relaxation times, where certain copolymer sequences with longer block lengths produce slower relaxations than even the pure B system. This suggests that adjusting copolymer sequence is potentially a powerful tool for controlling the material properties of nanocomposite systems even in cases where microphase separation does not occur in the bulk. In future work, we hope to study the effects of unfavorable interactions between unlike monomers as well as the effect of modeling two polymers with different glass transition temperatures, which would allow us to examine how copolymer sequence affects glass transition temperature in the interphase. It would also be of interest to extend our analysis to examine other monomer-nanoparticle interaction strengths, including those that are strong enough such that the adsorbing monomer type behaves as if grafted to the nanoparticle. Finally, we plan to examine the effect of copolymer sequence on other interphase properties, including entanglements, local dynamic modulus, and hysteresis in mechanical response.

## Conflicts of interest

There are no conflicts to declare.

## Acknowledgements

This work was improved by helpful discussions with Dr. Patrick Majors, and the authors thank Tarik Akyuz for developing portions of the local relaxation time analysis code. This material is based upon work supported by the National Science Foundation under Grant No. 1454343. The authors also thank the Cooper Tire and Rubber Company for funding a portion of this work and acknowledge the Ohio Supercomputing Center for providing an allocation of computing time.

## Notes and references

- 1 F. W. Starr, J. F. Douglas and S. C. Glotzer, *Journal of Chemical Physics*, 2003, **119**, 1777.
- 2 Y. Li, M. Kröger and W. K. Liu, *Physical Review Letters*, 2012, **109**, 118001.
- 3 Y. Li, M. Kröger and W. K. Liu, *Macromolecules*, 2012, **45**, 2099–2112.
- 4 F. W. Starr and J. F. Douglas, *Physical Review Letters*, 2011, **106**, 115702.
- 5 J. T. Kalathi, G. S. Grest and S. K. Kumar, *Physical Review Letters*, 2012, **109**, 198301.
- 6 Y. Song, M. Luo and L. L. Dai, *Langmuir*, 2010, **26**, 5–9.
- 7 P. J. Griffin, V. Bocharova, L. R. Middleton, R. J. Composto, N. Clarke, K. S. Schweizer and K. I. Winey, *ACS Macro Letters*, 2016, **5**, 1141–1145.
- 8 S. K. Kumar and R. Krishnamoorti, *Annual Review of Chemical and Biomolecular Engineering*, 2010, **1**, 37–58.
- 9 A. S. Sarvestani and E. Jabbari, *Macromolecular Theory and Simulations*, 2007, **16**, 378–385.
- 10 H. Chao and R. A. Riggleman, *Polymer*, 2013, **54**, 5222–5229.
- 11 R. C. Picu and A. Rakshit, *The Journal of Chemical Physics*, 2007, **126**, 144909.
- 12 T. Ge, J. T. Kalathi, J. D. Halverson, G. S. Grest and M. Rubinstein, *Macromolecules*, 2017, **50**, 1749–1754.
- 13 Y. N. Pandey, G. J. Papakonstantopoulos and M. Doxastakis, *Macromolecules*, 2013, **46**, 5097–5106.
- 14 V. Padmanabhan, A. L. Frischknecht and M. E. Mackay, *Macromolecular Theory and Simulations*, 2012, **21**, 98–105.
- 15 T. Chen, H.-J. Qian, Y.-L. Zhu and Z.-Y. Lu, *Macromolecules*, 2015, **48**, 2751–2760.
- 16 F. W. Starr, T. B. Schröder and S. C. Glotzer, *Macromolecules*, 2002, **35**, 4481–4492.
- 17 P. J. Dionne, C. R. Picu and R. Ozisik, *Macromolecules*, 2006, **39**, 3089–3092.
- 18 G. Maurel, F. Goujon, B. Schnell and P. Malfreyt, *The Journal of Physical Chemistry C*, 2015, **119**, 4817–4826.
- 19 A. Ghanbari, T. V. M. Nodoro, F. Leroy, M. Rahimi, M. C. Böhm and F. Müller-Plathe, *Macromolecules*, 2012, **45**, 572–584.
- 20 K. Johnston and V. Harmandaris, *Soft Matter*, 2013, **9**, 6696–6710.
- 21 K. Johnston and V. Harmandaris, *Macromolecules*, 2013, **46**, 5741–5750.
- 22 V. Ganesan, V. Pryamitsyn, M. Surve and B. Narayanan, *Journal of Chemical Physics*, 2006, **124**, 221102.
- 23 M. Wang and R. J. Hill, *Soft Matter*, 2009, **5**, 3940.
- 24 A. Ghanbari, M. Rahimi and J. Dehghany, *The Journal of Physical Chemistry C*, 2013, **117**, 25069–25076.
- 25 E. Voyiatzis, M. Rahimi, F. Müller-Plathe and M. C. Böhm, *Macromolecules*, 2014, **47**, 7878–7889.
- 26 S. Cheng, B. Carroll, V. Bocharova, J.-M. Carrillo, B. G. Sumpter and A. P. Sokolov, *The Journal of Chemical Physics*, 2017, **146**, 203201.
- 27 T. V. M. Nodoro, E. Voyiatzis, A. Ghanbari, D. N. Theodorou, M. C. Böhm and F. Müller-Plathe, *Macromolecules*, 2011, **44**, 2316–2327.
- 28 T. V. M. Nodoro, M. C. Böhm and F. Müller-Plathe, *Macromolecules*, 2012, **45**, 171–179.
- 29 N. Jouault, M. K. Crawford, C. Chi, R. J. Smalley, B. Wood, J. Jestin, Y. B. Melnichenko, L. He, W. E. Guise and S. K. Kumar, *ACS Macro Letters*, 2016, **5**, 523–527.
- 30 H. Mortazavian, C. J. Fennell and F. D. Blum, *Macromolecules*, 2016, **49**, 298–307.
- 31 S. Napolitano, E. Glynos and N. B. Tito, *Reports on Progress in Physics*, 2017, **80**, 036602.
- 32 H. Oh and P. F. Green, *Nature Materials*, 2009, **8**, 139–143.
- 33 Y. Song and Q. Zheng, *Progress in Materials Science*, 2016, **84**, 1–58.
- 34 H. M. Chen, Y. C. Jean, L. J. Lee, J. Yang and J. Huang, *physica status solidi c*, 2009, **6**, 2397–2400.
- 35 B. J. Ash, R. W. Siegel and L. S. Schadler, *Journal of Polymer Science Part B: Polymer Physics*, 2004, **42**, 4371–4383.
- 36 M. R. Bockstaller, R. A. Mickiewicz and E. L. Thomas, *Advanced Materials*, 2005, **17**, 1331–1349.

- 37 B. Dong, R. Guo and L.-T. Yan, *Macromolecules*, 2014, **47**, 4369–4379.
- 38 Q. Zhang, L. Zhang and J. Lin, *The Journal of Physical Chemistry C*, 2017, **121**, 23705–23715.
- 39 P. Chen, Y. Yang, B. Dong, Z. Huang, G. Zhu, Y. Cao and L.-T. Yan, *Macromolecules*, 2017, **50**, 2078–2091.
- 40 R. Liang, J. Xu, W. Li, Y. Liao, K. Wang, J. You, J. Zhu and W. Jiang, *Macromolecules*, 2015, **48**, 256–263.
- 41 Z. Huang, P. Chen, Y. Yang and L.-T. Yan, *The Journal of Physical Chemistry Letters*, 2016, **7**, 1966–1971.
- 42 K. J. Modica, T. B. Martin and A. Jayaraman, *Macromolecules*, 2017, **50**, 4854–4866.
- 43 C. E. Estridge and A. Jayaraman, *The Journal of Chemical Physics*, 2014, **140**, 144905.
- 44 A. Jayaraman, *Journal of Polymer Science Part B: Polymer Physics*, 2013, **51**, 524–534.
- 45 M. Tagliazucchi, O. Peleg, M. Kröger, Y. Rabin and I. Szleifer, *Proceedings of the National Academy of Sciences*, 2013, **110**, 3363–3368.
- 46 S. Ohta, D. Glancy and W. C. W. Chan, *Science*, 2016, **351**, 841–845.
- 47 H.-m. Ding and Y.-q. Ma, *Small*, 2014, **11**, 1055–1071.
- 48 H. Chen and E. Ruckenstein, *Langmuir*, 2014, **30**, 3723–3728.
- 49 T. Martin, C. McKinney and A. Jayaraman, *Soft Matter*, 2013, **9**, 155–169.
- 50 D. Banerjee and K. S. Schweizer, *Journal of Polymer Science Part B: Polymer Physics*, 2015, **53**, 1098–1111.
- 51 D. Banerjee, M. Dadmun, B. Sumpter and K. S. Schweizer, *Macromolecules*, 2013, **46**, 8732–8743.
- 52 L. M. Hall and K. S. Schweizer, *Macromolecules*, 2011, **44**, 3149–3160.
- 53 E. Helal, L. Amurin, D. Carastan, R. de Sousa, E. David, M. Fréchet and N. Demarquette, *Polymer*, 2017, **113**, 9–26.
- 54 A. J. Trazkovich, T. H. Akyuz and L. M. Hall, *Tire Science and Technology*, (in press), year.
- 55 K. Kremer and G. S. Grest, *The Journal of Chemical Physics*, 1990, **92**, 5057–5086.
- 56 G. S. Grest, M.-D. Lacasse, K. Kremer and A. M. Gupta, *The Journal of Chemical Physics*, 1996, **105**, 10583–10594.
- 57 R. S. Hoy, K. Foteinopoulou and M. Kröger, *Physical Review E*, 2009, **80**, 031803.
- 58 K. Sugiyama, T. Oie, A. A. El-Magd and A. Hirao, *Macromolecules*, 2010, **43**, 1403–1410.
- 59 J. Liu, Y. Wu, J. Shen, Y. Gao, L. Zhang and D. Cao, *Physical Chemistry Chemical Physics*, 2011, **13**, 13058–13069.
- 60 W. Shinoda, M. Shiga and M. Mikami, *Phys. Rev. B Physical Review B*, 2004, **69**, year.
- 61 J. V. Heffernan, J. Budzien, F. Avila, T. C. Dotson, V. J. Aston, J. D. McCoy and D. B. Adolf, *The Journal of Chemical Physics*, 2007, **127**, 214902.
- 62 J. Sampath and L. M. Hall, *Soft Matter*, 2018, **14**, 4621–4632.

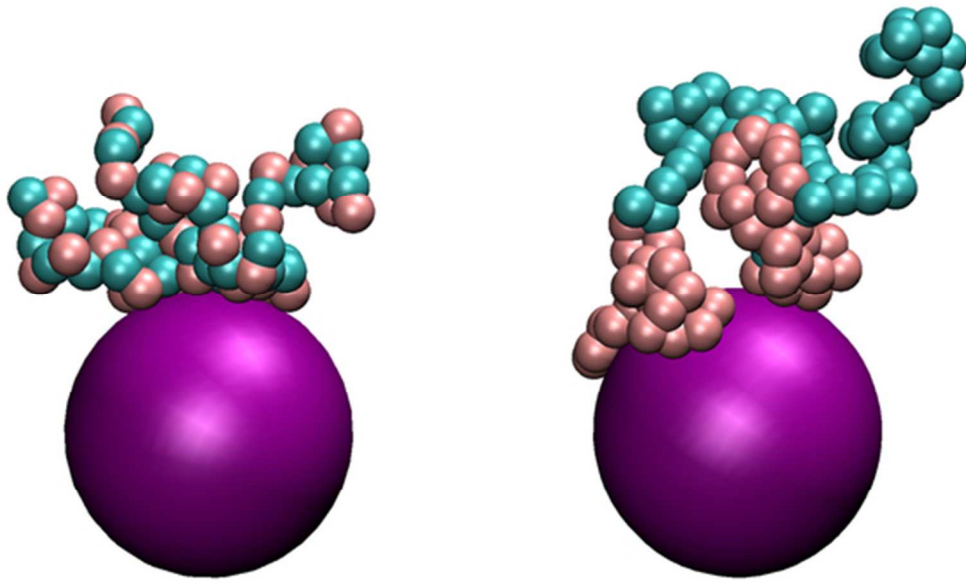


Fig. 1

48x28mm (300 x 300 DPI)

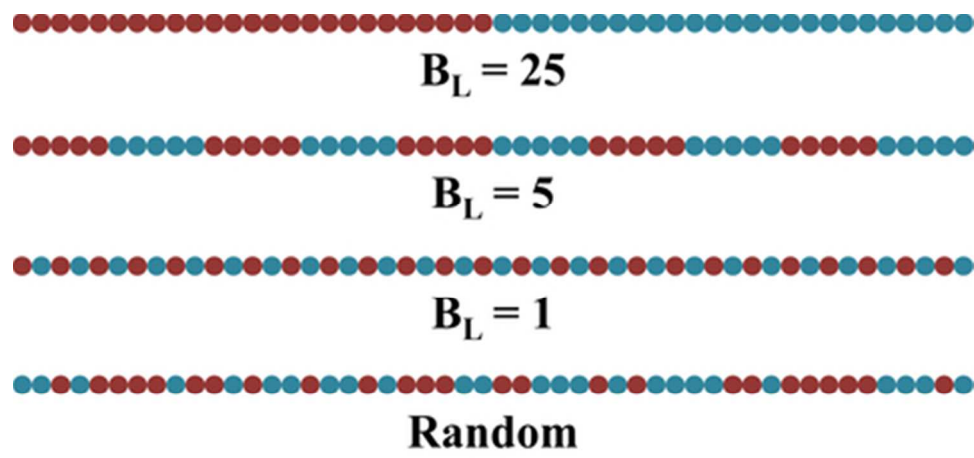


Fig. 2

40x19mm (300 x 300 DPI)

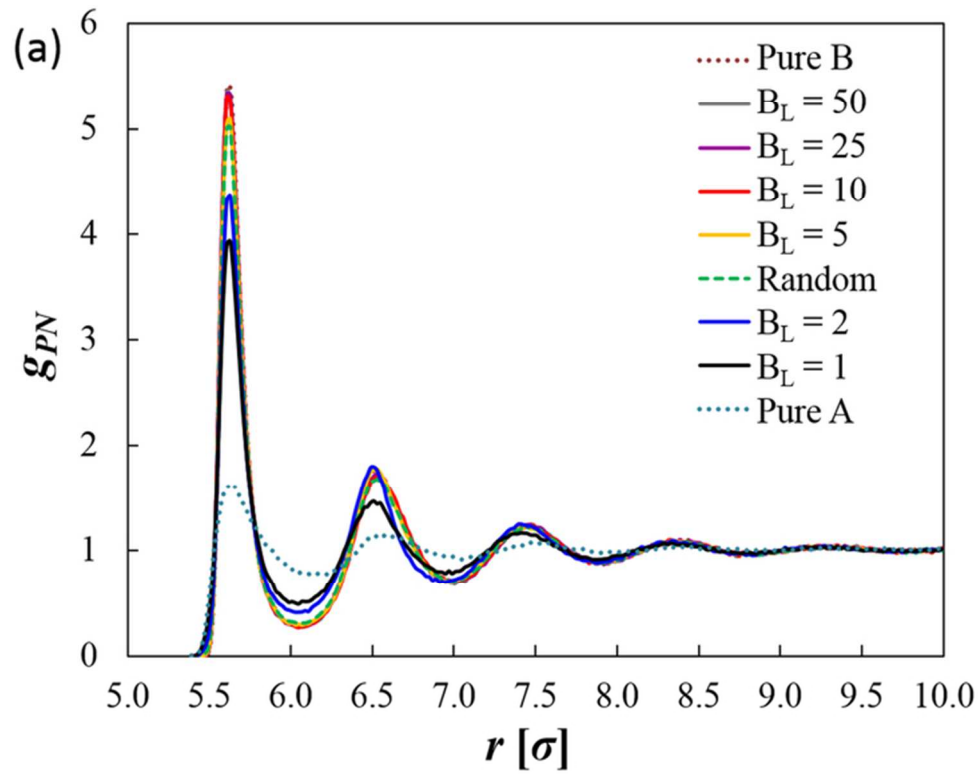


Fig. 3a

63x48mm (300 x 300 DPI)

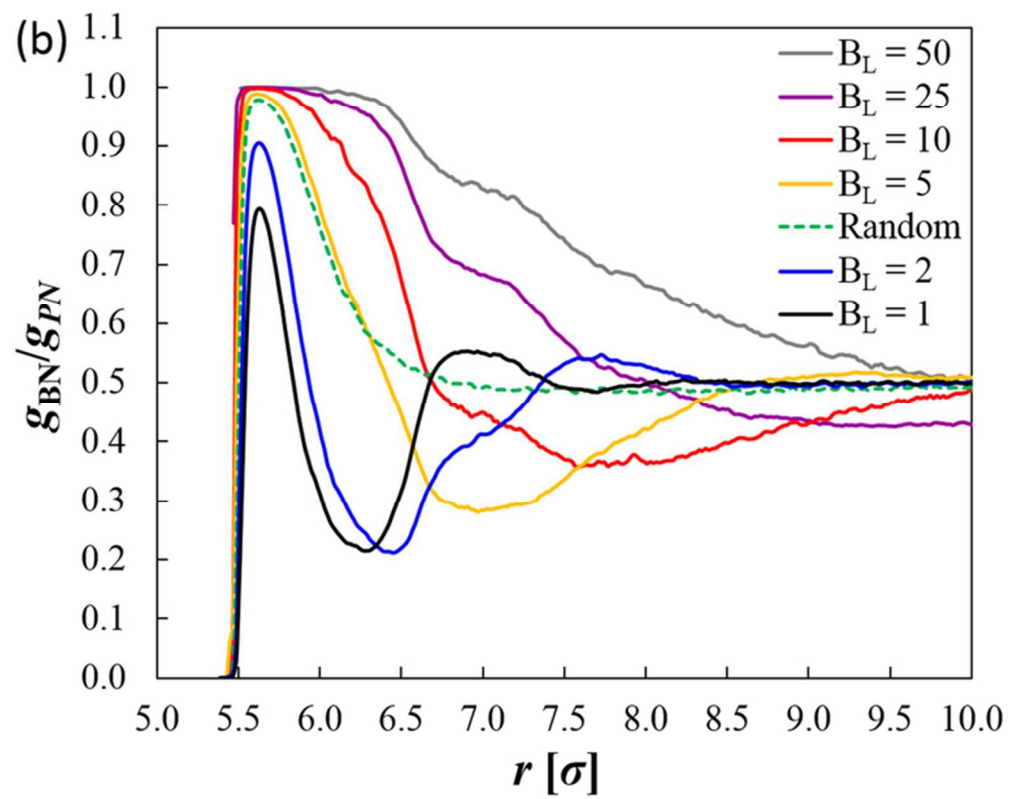


Fig. 3b

65x51mm (300 x 300 DPI)

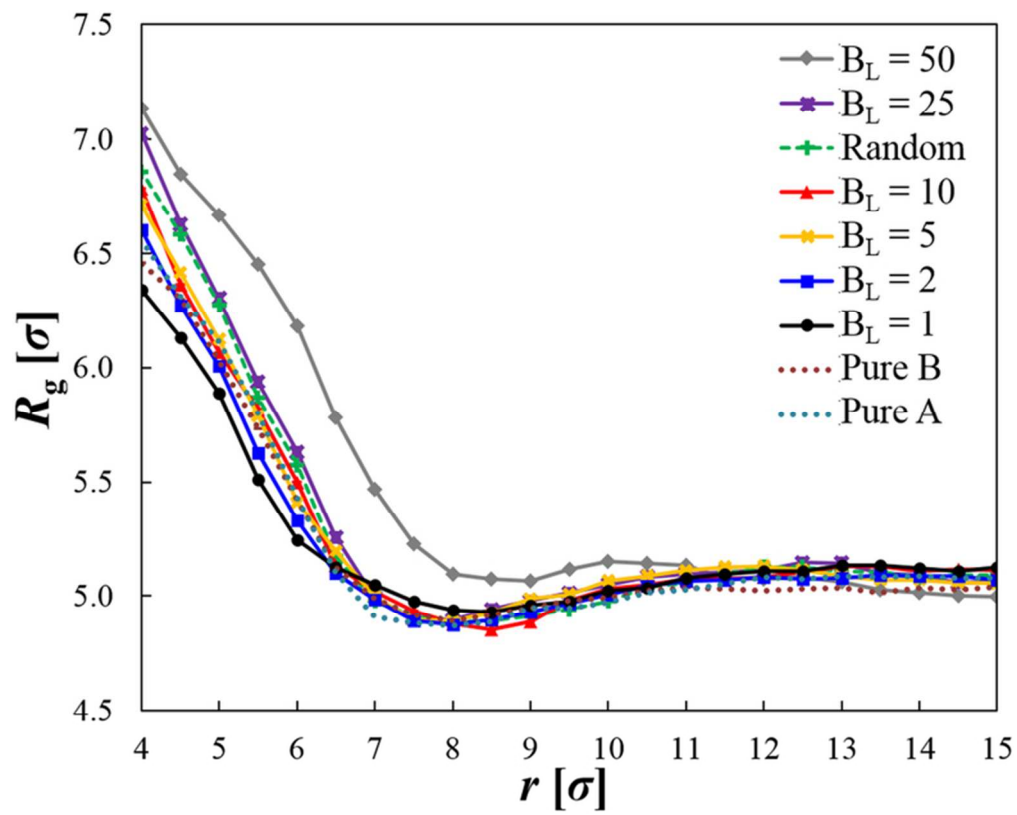


Fig. 4

66x53mm (300 x 300 DPI)

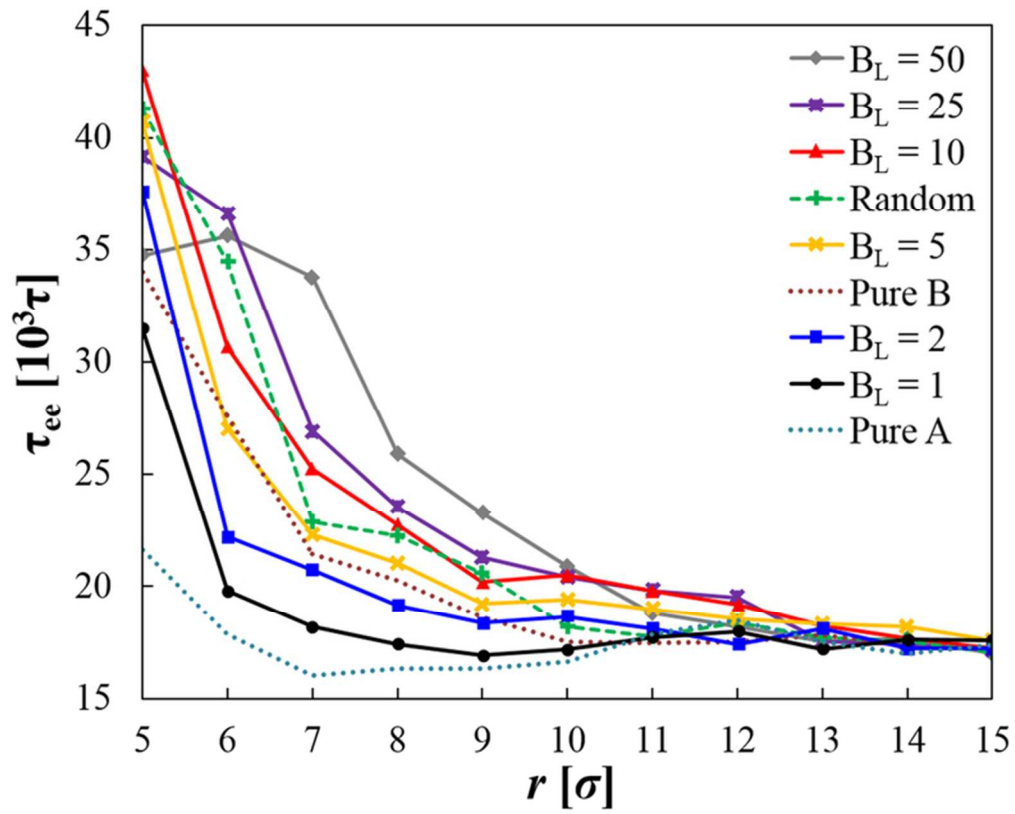


Fig. 5

66x53mm (300 x 300 DPI)

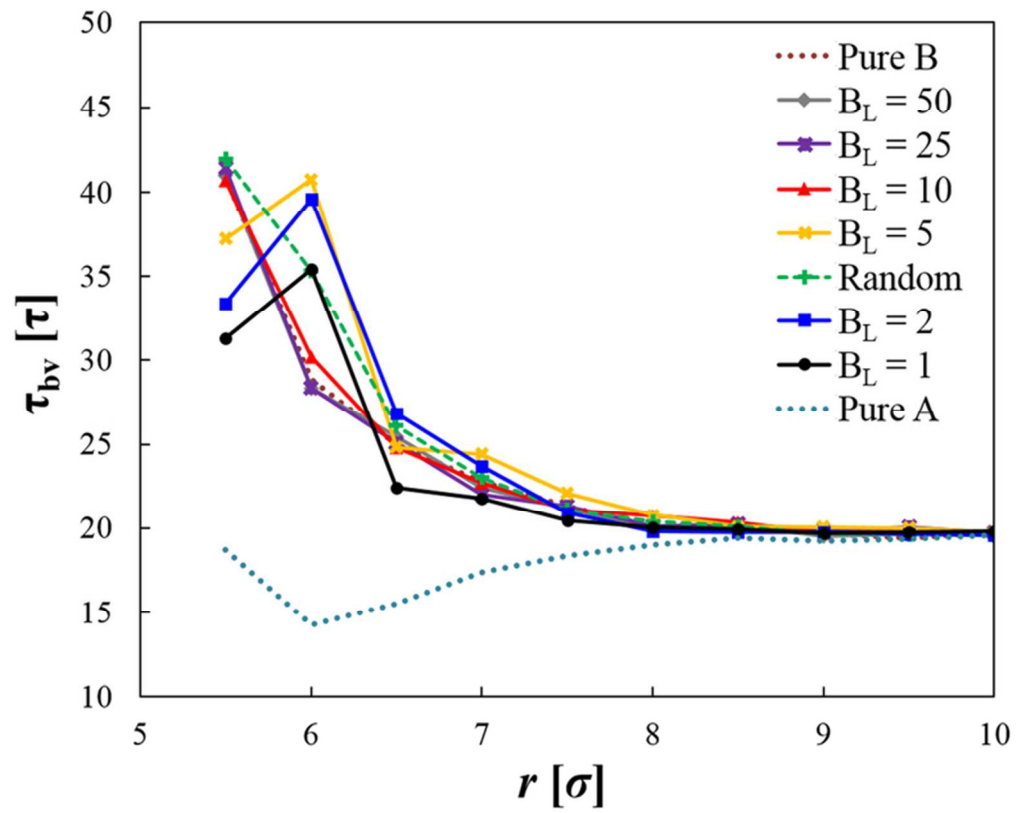


Fig. 6

66x52mm (300 x 300 DPI)

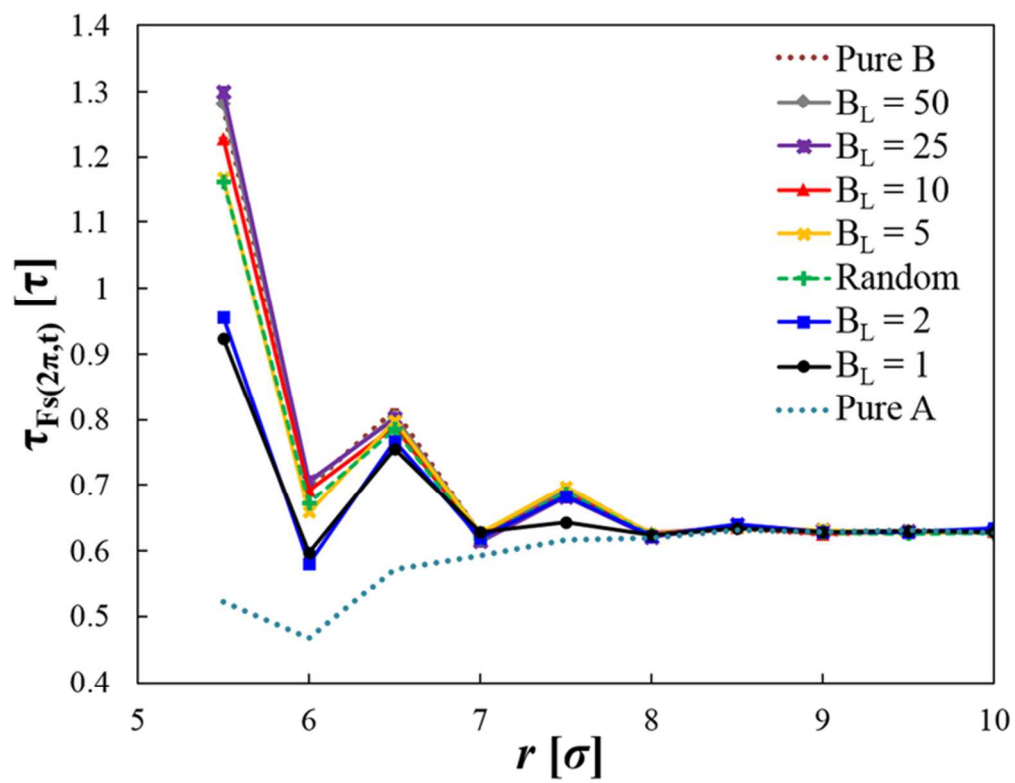
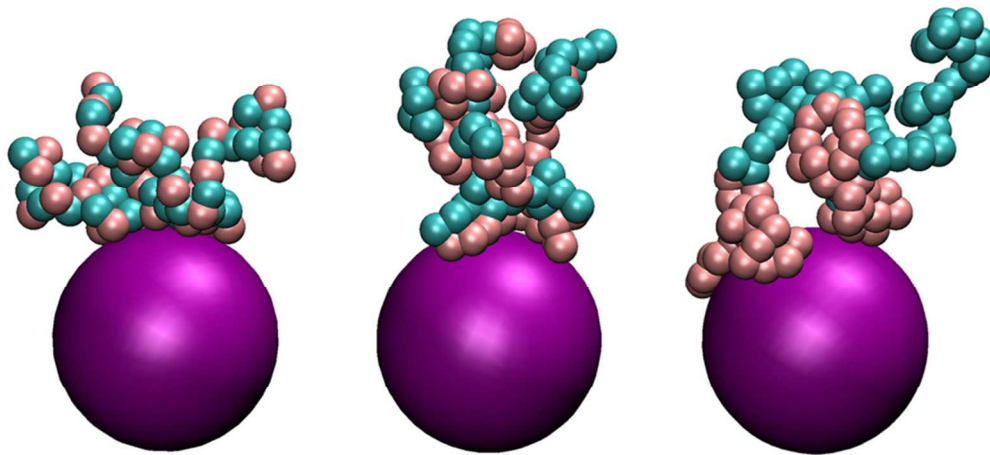


Fig. 7

63x49mm (300 x 300 DPI)



Copolymer sequence affects the size and dynamics of the interphase region around a nanoparticle.

40x20mm (600 x 600 DPI)